ISSN 1345-3041

Dec.2024 / Vol.188

Mitsubishi Electric

ADVANCE

Advanced Digital Technology (The first part)

MITSUBISHI ELECTRIC
Changes for the Better

December 2024 / Vol. 188

Mitsubishi Electric

ADVANCE

Advanced Digital Technology (The first part)

• **Editorial Inquiries**
Fumitoshi Yoshikawa
Corporate Productivity Planning & Engineering Dept.
Fax: +81-3-3218-2465

Mitsubishi Electric Advance is published on line quarterly (in March, June, September, and December) by Mitsubishi Electric Corporation.

CONTENTS

Overview

Technical Reports

Precis

Our aim in the Mitsubishi Electric Group is to be a “Circular Digital-Engineering” company, and we are working to solve increasingly severe and diverse social problems through innovation based on advanced digital technology. In this way, we hope to contribute to the realization of a dynamic, yet relaxed and fulfilling society. For this special feature, we will present specific initiatives in the area of advanced digital technology across two issues: a first part (this issue, ADVANCE Vol. 188, December 2024) and a second part (the next issue, Vol. 189, March 2025).

Overview

Author: *Toru Oka**

**Executive Officer, In charge of Intellectual Property,
Vice President, Corporate Research and Development*

Advanced Digital Technology Contributing to Solution of Social Issues

As a “Circular Digital-Engineering” company, Mitsubishi Electric Group is working to achieve a higher level of value through the use of advanced digital technologies. By creating value through Circular Digital-Engineering and innovation, we will strive to make a “Trade-On” (mutual benefits) between business growth and enriching society and the environment, and achieve sustainability by contributing to a sustainable society by solving social issues through our business.

In Circular Digital-Engineering, we consolidate and analyze data obtained from customers in a digital space. By leveraging strong intra-group connections and knowledge sharing, we create new value and contribute to the solution of social problems.

Creating new value requires technology to realize services and products, as well as technology that enables them to be used safely. Therefore, as we develop technologies for individual products and services, we are also developing advanced digital technologies in areas such as security and privacy protection to ensure worry-free, safe use of AI. In the December and March issues of Mitsubishi Electric ADVANCE, we will present specific initiatives in these areas.

At the Mitsubishi Electric Group, we aim to be a “Circular Digital-Engineering” company and will use innovation based on advanced digital technologies to address increasingly serious and diverse social issues and contribute to the realization of a vibrant and sustainable society.

Maximization of Sensitivity to Time-series Polarimetric SAR Image

Author: *Motofumi Arii**

**Information Technology R&D Center*

Abstract

Understanding the earth's day-to-day changes is an urgent issue for humanity as part of efforts to address global climate change and support recovery from disasters. Synthetic Aperture Radar (SAR) is a technology Mitsubishi Electric has been developing for many years. SAR enables observation day or night, regardless of weather, and is outstanding for detecting, through periodic observation, changes in the earth's surface as differences. Furthermore, Polarimetric SAR (PolSAR) images utilizing the polarization of the SAR transmitting/receiving antennas enable estimation of aspects such as the structure and materials of the observation targets. Mitsubishi Electric has developed a technology for boosting sensitivity to changes in the state of the target, based on PolSAR images observed in a time series, and achieving quantitative measurement without missing even slight differences. We have shown it is possible to quantitatively measure seasonal changes in broad-leaved forests in Hokkaido by applying this technique to PolSAR images taken with the second Advanced Land Observation Satellite (ALOS-2).

1. Introduction

When observing earth from space, day-to-day relative changes obtained from time-series images utilizing orbit recurrence are more important than absolute changes obtained from single observations. Unlike an optical camera, SAR is capable of observation day or night, regardless of weather, and if there is no change in the observation target on the earth, there is a high probability that the same power can be received (reproducibility). In addition, sensitivity to the form and material of the observation target is improved by switching polarization characteristics while transmitting and receiving. The PolSAR installed in satellites is particularly outstanding at capturing subtle changes in the earth's surface. Mitsubishi Electric has been involved in the development of all previous satellites equipped with PolSAR functionality by the Japan Aerospace Exploration Agency (JAXA) (Fig. 1). The greatest advantage of PolSAR observation is that once observation is done with two orthogonal polarizations, it is possible to reproduce, offline, the received power corresponding to any transmission/reception polarization. Our company looked again at this basic characteristic of PolSAR images, and developed a technology for quantitatively measuring tiny changes in the observation target with an unprecedented sensitivity.

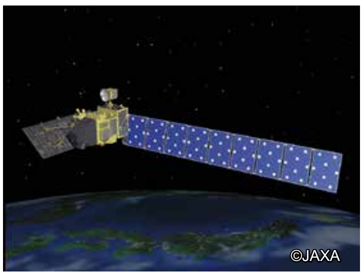

ALOS-1

ALOS-2

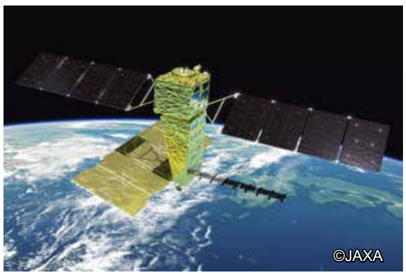

ALOS-4

Fig. 1 PolSAR satellites

2. Received Power of PolSAR

Polarization, a fundamental property of electromagnetic waves, is the regular behavior of electric and magnetic fields in a plane perpendicular to the direction of propagation. Such electromagnetic waves are called polarizations and generally have an elliptical shape (Fig.2). In Fig. 2, the propagation direction is perpendicular to the paper surface.

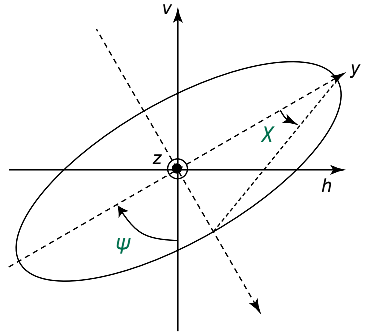

Fig. 2 Orientation angle ψ and ellipticity angle χ of an electromagnetic wave

The polarization state $\vec{p}$ can be expressed as follows using as variables the orientation angle ψ and the ellipticity angle χ that characterize the ellipse.

$$\vec{p}^{\,i} = \begin{pmatrix} p_h^i \\ p_v^i \end{pmatrix} = \begin{bmatrix} \cos\psi^i & \sin\psi^i \\ -\sin\psi^i & \cos\psi^i \end{bmatrix} \begin{bmatrix} j\sin\chi^i \\ \cos\chi^i \end{bmatrix} \quad i = t, r \quad \cdots\cdots (1)$$

Where, t and r stand for transmission and reception, and polarization states can be specified, respectively, for the transmission antenna and reception antenna that constitute the radar equipment (Fig. 3). "v_1, v_2, ..." in Fig. 3 indicate physical quantities of the observation target (such as soil moisture or the plant growth situation).

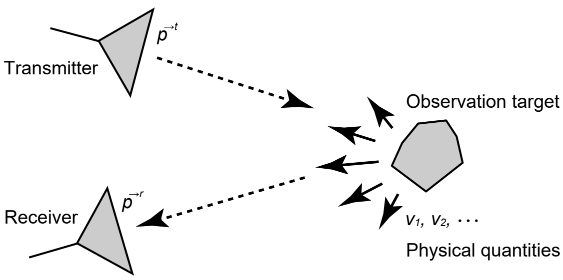

Fig. 3 PolSAR observation

That is, the polarization state used for observation can be specified with four variables (ψ^t, χ^t, ψ^r, and χ^r). Horizontal polarization and vertical polarization (Fig. 4) are widely used in actual PolSAR observation, and observation is performed while successively switching the polarization state during transmission and reception.

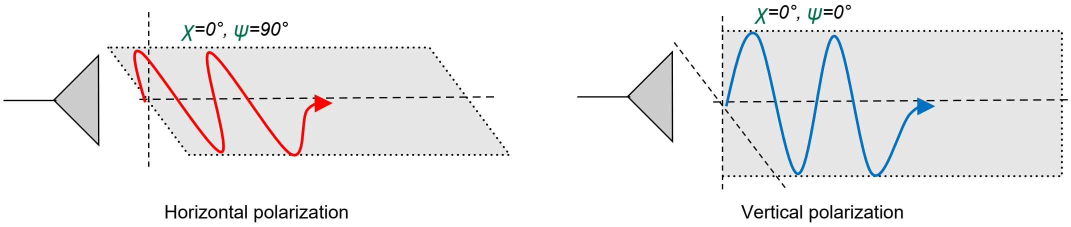

Fig. 4 Orthogonalized polarization waves

For example, signals obtained by transmitting vertical polarizations and receiving the scattering from the observation target as horizontal polarizations are called HV polarizations. Through PolSAR observations, HH, HV, VH, and VV polarizations (hereinafter referred to as "standard polarizations") are recorded. Previous SAR only recorded one of these polarizations. The received power P can be described using a four-dimensional antenna vector $\vec{A}$ consisting of (ψ^t, χ^t, ψ^r, χ^r) representing the transmission and receipt polarization states and a 4x4 covariance matrix C consisting of the radio scattering information from the observation target, as follows:

$$P=\vec{A}(\vec{p}^{\,t}(\psi^t,\ \chi^t),\ \vec{p}^{\,r}(\psi^r,\ \chi^r))^T C(v_1, v_2, \cdots)\vec{A}(\vec{p}^{\,t}(\psi^t,\ \chi^t),\ \vec{p}^{\,r}(\psi^r,\ \chi^r))^* \quad \cdots\cdots\cdots\cdots\cdots (2)$$

The scalar P can be regarded as the brightness of each pixel of the PolSAR image. The covariance matrix constructed through observation can be visualized by the polarization signature(1). Here, visualization was done (Fig. 5) by successively calculating P while varying ψt and χt, for the case where the polarization state is the same for transmission and reception (Co-Pol) ($\vec{p}^{\,t} = \vec{p}^{\,r}$), and the case where they are orthogonal (Cr-Pol) ($\vec{p}^{\,t} \cdot \vec{p}^{\,r} = 0$).

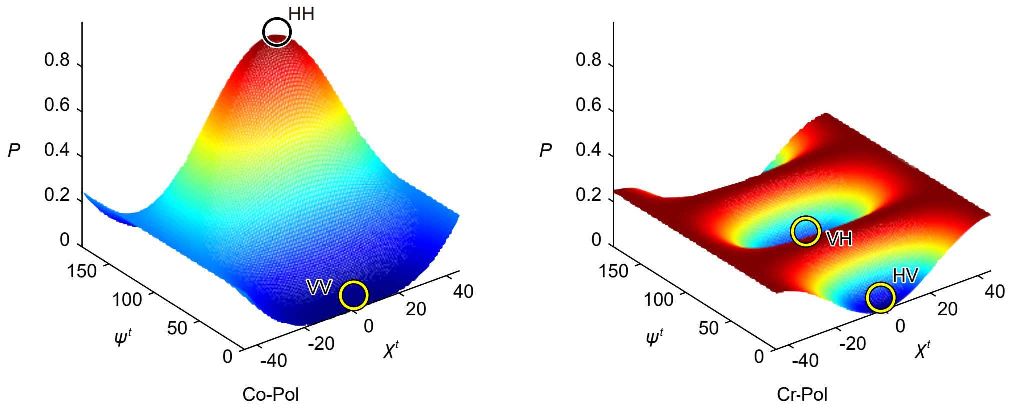

Fig. 5 Polarization signature of 90°oriented dipole

The standard polarizations are the powers corresponding to the four points in Fig. 5. In previous SAR, only one of these points was observed. However, the covariance matrix obtained with PolSAR contains a great deal of information besides that. This means that once a covariance matrix is constructed with two orthogonal polarizations, it is possible in principle to reproduce the power of any transmission-reception polarization state. This property is the one of the most important features of PolSAR. For example, it has been used as a technique for emphasizing contrast of two observation targets (e.g., ships vs. the ocean surface) in the same image(2). In this paper, the property is applied to high-sensitivity detection of quantitative change in time-series PolSAR images. In Fig. 5, the maximum power just happens to be captured by the HH polarization (χ^t=0°, χ^t=90°) but that depends on the condition of the observation target and is not always the case.

3. Technique for Maximizing Sensitivity to Differences

The discussion in this section 3 is based on PolSAR images of two scenes with different observation times. The power difference due to the change in state of the observation target during this period can be described as follows.

$$\Delta P=P(t_1)-P(t_0)=\vec{A}(\psi^t,\ \chi^t,\ \psi^r,\ \chi^r)^T\{C(t_1)-C(t_0)\}\vec{A}(\psi^t,\ \chi^t,\ \psi^r,\ \chi^r)^* \quad \cdots\cdots\cdots\cdots\cdots (3)$$

This shows that the power difference can be maximized, in the following way, by appropriately selecting $\vec{A}$, provided there is a change in the observation target.

$$(\psi^t_{opt},\ \chi^t_{opt},\ \psi^r_{opt},\ \chi^r_{opt}) = \max_{\psi^t,\chi^t,\psi^r,\chi^r}\left|\frac{\partial P(\psi^t,\ \chi^t,\ \psi^r,\ \chi^r,\cdots)}{\partial t}\right| \quad \cdots\cdots\cdots\cdots\cdots (4)$$

The optimal polarization state can be found by applying the method of Lagrange multiplier.

To illustrate the specific processing method based on this principle, the following example shows a case where the same region was observed four times during the period from t_0 to t_3 (Fig. 6).

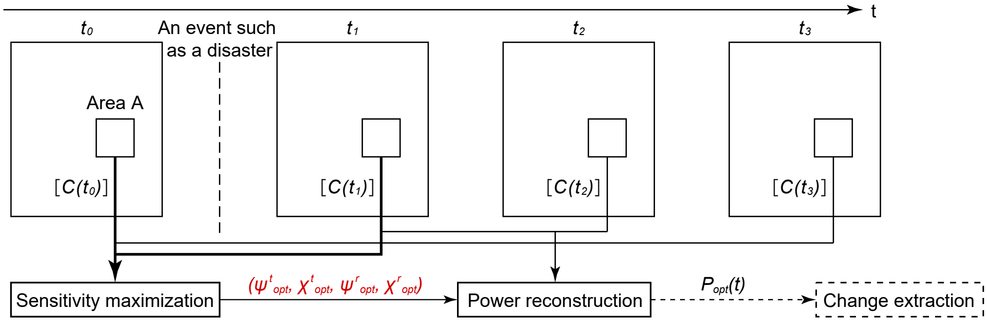

Fig. 6 Algorithm of a maximization of polarimetric sensitivity

It is assumed that, in the interval between t_0 and t_1, a major change occurs due to an event such as a disaster, and after that there is a gradual recovery at t_2 and t_3, First, the optimal angles that maximize the difference (ψ^t_{opt}, χ^t_{opt}, ψ^r_{opt}, χ^r_{opt}) are found from the PolSAR images for t_0 and t_1, where change is the greatest, and these are stored for each pixel. Next, the power at each time is reconstructed by applying the stored optimal angles to Equation(2) in section 2. By using the same antenna vector $\vec{A}$ (ψ^t_{opt}, χ^t_{opt}, ψ^r_{opt}, χ^r_{opt}) in all periods in this way, it is possible to establish a standard for comparing change, and the change in the target can be localized to $|C(t_1)-C(t_0)|$. The differences between arbitrary images from the four reconstructed PolSAR images enable quantitative analysis as changes in the state of the target. On the other hand, the optimal angle itself can be a new physical parameter representing the state of the observation target.

4. Validation: Maximizing Sensitivity to Forest Growth

ALOS-2 was used to observe the broad-leaved forest in Tomakomai City in Hokkaido at three times (t_0: December 30, 2018; t_1: January 27, 2019; and t_2: August 11, 2019). The technique examined in section 3 was applied to those PolSAR images. As is evident in the photos in Fig. 7, there are conspicuous time series changes characteristic of deciduous trees.

March 2015

June 2016

Fig. 7 Snapshots taken in deciduous forest of Tomakomai

Figure 8 shows HH polarization images of the same region. From t_0 to t_1, there is only the difference of one month in the winter season, just a small change, But from t_1 to t_2, there is a marked increase in brightness due to leaf growth from winter to summer.

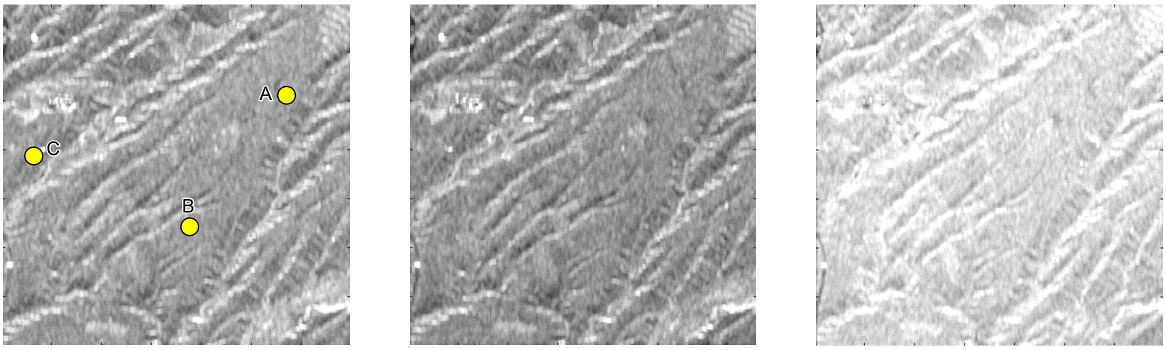

(a) t_0 (December 30, 2018) (b) t_1 (January 27, 2019) (c) t_2 (August 11, 2019)

Fig. 8 Time-series PolSAR images obtained by ALOS-2 (HH)

Here, sensitivity is maximized for t_0 and t_2, where the maximum change is expected. For locations A to C indicated in Fig. 8(a), the results of power reconstruction after sensitivity maximization are shown in Fig. 9. To emphasize sensitivity, Fig. 8(b) and (c) are shown as the power difference at an arbitrary time and t_0.

At all locations, received power shows an increasing trend in accordance with growth. Valid results are obtained, with the reconstructed power (P_{OPT}) becoming maximal at t_2, and exhibiting natural changes including t_1. This technique enables quantitative analysis of physical changes in the target region, based on differences of arbitrary pairs, because the standard for comparison during the period is the same.

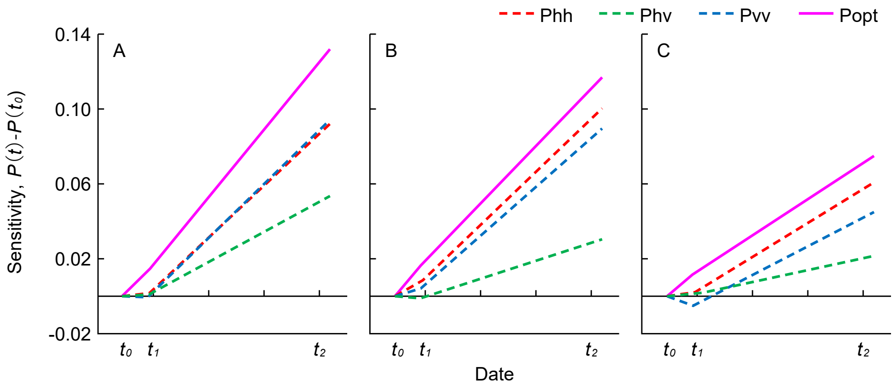

Fig. 9 Time histories of the received power and its sensitivity in areas A–C of Fig. 8(a)

To validate this technique for the entire image, Fig. 10 shows the difference images of t_0 and t_2 after power reconstruction.

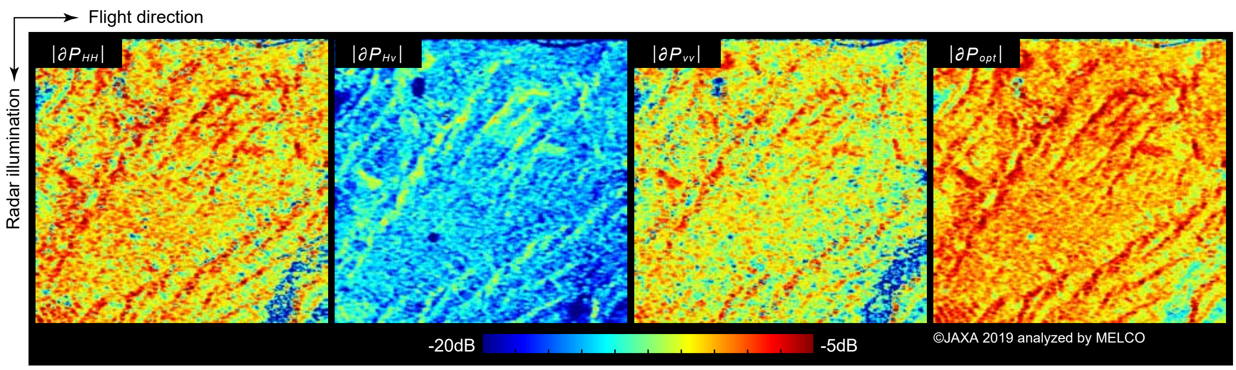

(a) HH polarization (b) HV polarization (c) VV polarization (d) Difference image after difference maximization

Fig. 10 Comparison of optimized difference map (right) with those of standard polarizations between t_0 and t_2

The HH image (Fig. 10(a)) is the difference of Fig. 8(a) t_0 and (c) t_2. It is evident that, over the entire range of the image, the magnitude of the change due to the proposed technique (Fig. 10(d)) is maximal. Also, the angle formed by the transmission-reception polarization state is defined as follows, taking the obtained optimal angle as a new physical quantity.

$$cos\gamma_{opt} = \frac{\vec{p}^{\,t}_{opt} \cdot \vec{p}^{\,r}_{opt}}{|\vec{p}^{\,t}_{opt}|\,|\vec{p}^{\,r}_{opt}|} \quad \cdots\cdots\cdots (5)$$

Histograms of ψ_{opt}, χ_{opt}, and γ_{opt} in the image range of the ALOS-2 image (Fig. 8) are shown in Fig. 11.

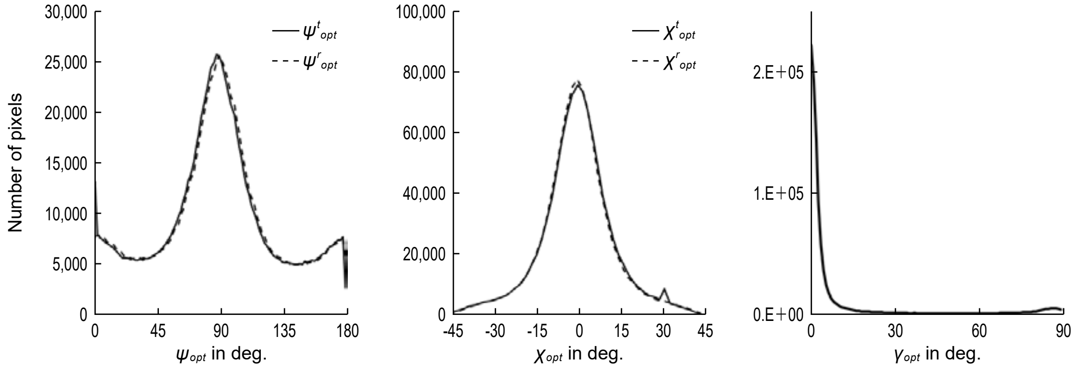

Fig. 11 Histograms of optimized polarimetric angles ψ_{opt} (left), χ_{opt} (center), and γ_{opt} (right) of ALOS-2 image of Fig. 8

ψ_{opt} and χ_{opt} exhibit almost equal distributions in transmission and reception, and respectively have mean values near 90° (horizontal polarization) and 0° (linear polarization). For γ_{opt}, it was shown quantitatively that almost all pixels indicate 0° (transmission and reception polarization state are equal), and for the pertinent region as a whole, sensitivity is high near HH polarization (90°), but there is also a considerable distribution at other orientation angles.

5. Conclusion

This paper describes a technique used with PolSAR images to maximize time series sensitivity and quantitatively measure changes in arbitrary observation targets. The proposed technique was applied to PolSAR images observed in time series with ALOS-2, and it was confirmed that differences can be maximized. It was also shown that more various information for each observation target can be extracted by using the optimal polarization state itself that is obtained for each pixel. Mitsubishi Electric will apply this technology to the monitoring of forest growth for global warming countermeasures and the extraction of disaster areas caused by flooding due to linear precipitation zones, which have been rapidly increasing in recent years. By combining this technology with the PolSAR satellite development technology we have cultivated over the years, Mitsubishi Electric will continue to provide technology that enables quantitative and precise understanding of global changes in the earth's surface on a global scale.

References

(1) Jakob, J. van Zyl: On the Importance of Polarization in Radar Scattering Problems, Ph. D. Thesis, California Institute of Technology (1985)
(2) Swartz, A. A., et al.: The Optimal Polarizations for Achieving Maximum Contrast in Radar Images, Journal of Geophysical Research, 93, No.B12, 15252–15260 (1988)

Low Power Design of Real-Time Forward Error Correction Circuit Based on the Characteristics of State-of-the-Art Processes

Authors: *Kenji Ishii*, Hideo Yoshida**

**Information Technology R&D Center*

Abstract

In realizing a digital society, we cannot avoid the issues of increasing the speed of digital signal processing and lowering its power consumption. To simultaneously achieve these contradictory characteristics, it is important not only to make advances in digital signal processing technology and integration technology made possible by the miniaturization of semiconductor processes, but also to develop low-power digital design techniques that take into account the characteristics of systems and applications. This paper describes low-power design technology that applies advanced wafer manufacturing processes, using the development of error-correction circuits for large-capacity optical communications as an example. Circuit design with high feasibility was achieved by optimizing the code and circuit architecture based on physical synthesis results assuming process characteristics, and power reduction effectiveness exceeding 40% was obtained, relative to maximum operation, through circuit control taking into account characteristics in terms of equipment operation.

1. Introduction

Social transformation continues to move forward, based on digital technologies exemplified by Digital Transformation (DX). Increasing the capacity of digital signal processing, and reducing its power consumption, are perennial topics in the use of such digital technology. In the optical communication industry, systems exceeding 400Gbps are being introduced to cope with growing traffic demand, and R&D is being conducted to further increase speed to 800Gbps and beyond. The improvement in communication speed is largely due to developments in signal processing technology, including error-correction technology, and integration technology resulting from the miniaturization of semiconductor processes. Previously, progress has been made in increasing capacity through parallelization and improved operating frequencies, while also reducing power consumption through process miniaturization. However, in recent years, the improvement of operating frequency has reached its limit, and in order to achieve high-speed processing, there is no choice but to rely on parallel processing. Since the effect of reducing power consumption by process miniaturization is small compared to the increase in power consumption due to parallelization, it is becoming difficult to meet the power consumption requirements. In particular, since the power consumption of error-correction circuits accounts for a large proportion of the power consumption within the device, reducing the power consumption has become increasingly important in recent years. In this paper, we first outline the forward error correction code circuit that is the target of power saving, and then describe the power saving technology we have developed from the perspectives of circuit element implementation and algorithm processing.

2. Technical Trends of Forward Error Correction Codes for Optical Communications

In optical communication networks, Low-Density Parity-Check (LDPC) codes, which have excellent correction capabilities, are often used as forward error correction codes to achieve error-free, large-capacity transmission over long distances. LDPC codes were proposed by Gallager in the 1960s[1] and have recently been adopted in standards for satellite digital broadcasting and wireless communications. This section explains these LDPC codes.

2.1 LDPC codes

LDPC codes are codes defined by a sparse parity check matrix (many “0” s and few “1” s) and are known to achieve high error-correction performance. Figure 1 shows an example of a check matrix and its representation as a bipartite graph. With an LDPC code, errors are corrected by propagating beliefs using the connection relationships of the graph. The distinguishing features of this decoding processing are that it is suitable for parallel processing by hardware, and it enables circuit implementation with high throughput. However, LDPC codes with practical code length are connected irregularly due to the huge amount of Tanner graph wiring, and thus the difficulty of decoding circuit implementation is extremely high. Therefore, it is important to design check matrices with high error-correction performance and circuit feasibility.

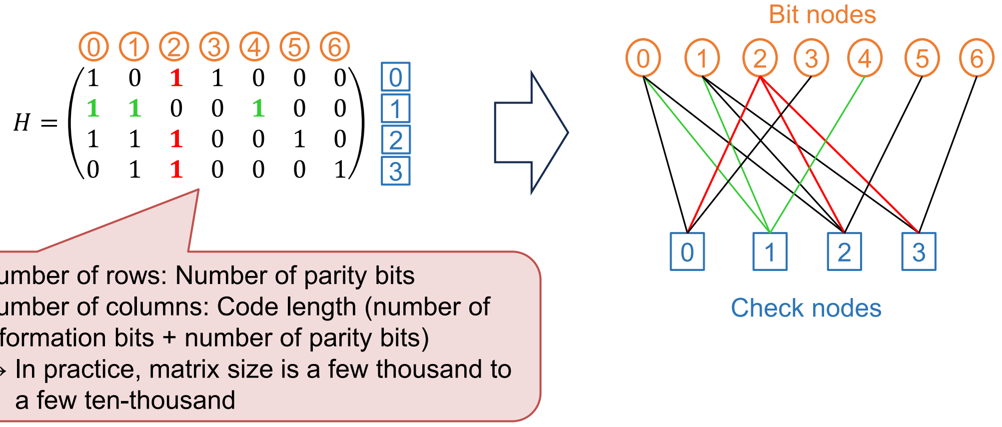

Fig. 1 Example of a parity check matrix and its Tanner graph

2.2 Quasi-Cyclic LDPC

Quasi-Cyclic (QC) LDPC codes are being considered as codes having both good error-correction performance and circuit implementability. With QC-LDPC codes, non-zero components of the parity-check matrix are constructed with circulant matrices obtained by circular shifts of the unit matrix. Figure 2 shows the configuration of a decoding circuit for a QC-LDPC code If 1s are arranged at random in the parity-check matrix of an LDPC code, then anywhere from several thousand to several ten-thousand core modules for decoding operations (row operation cores, column operation cores) are arranged directly below the first level, and since each of these is irregularly connected, it becomes a hotbed for wiring congestion and timing violations. However, by adopting the configuration of a QC-LDPC code, it is possible to consolidate operation blocks in circulant matrix size units, and this enables circuit optimization and layout adjustment in block units. In QC-LDPC code design, the size of the circulant matrices and their shift amounts are also important parameters, and optimization is necessary to coordinate with the decoding circuit architecture and process rules.

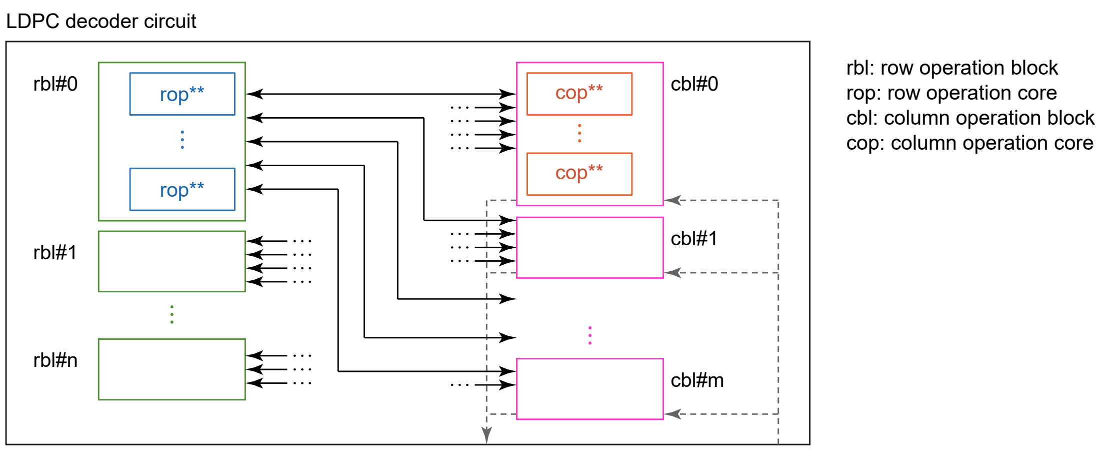

Fig. 2 QC-LDPC code decoder configuration example

3. Search for a QC-LDPC Code and Decoding Circuit Architecture Taking Circuit Characteristics into Account

Even if a QC-LDPC code is suitable for development as a circuit, the difficulty of layout design is still high, and trial-and-error is necessary to meet the required specifications. In the wafer manufacturing process in recent years, cell units have become smaller, and convergence of wiring onto those smaller cells has led to wiring congestion, and a greater tendency for timing violations to occur due to wiring delays for the purpose of avoiding congestion. The easiest way to resolve timing violations is to use high-speed cells provided for the purpose of increasing circuit speed, but these cells have the disadvantage of high power consumption. Also, cell characteristics fluctuate due to variability, voltage, temperature, and operating frequency, and conditions vary due to process rules, so the circuit architecture must be optimized to suit the applied process, code, and decoding algorithm[2]. Furthermore, the parity-check matrix has an effect not only on error-correction performance but also on circuit scale, and thus feedback design, where code design is based on decoding circuit physical synthesis results, is also necessary.

Table 1 shows trial results of design optimization for an error-correction circuit with 800Gbps throughput for an optical communication Application Specific Integrated Circuit (ASIC). With this design, the goal was to achieve the target performance from the standpoint of both code design and circuit design. With Method 1, goals were met for error-correction performance and power consumption, but timing violations and wiring congestion occurred, and the result had low feasibility. With Method 2, a pipeline approach was used

Table 1 Circuit design results for 800Gbps throughput forward error-correction decoder

Method	Overview of revision content	Code (Circulant matrix size)	Correction performance	Power Consumption (W) (800Gbps)	Soft-decision decoding circuit gate count (MG)	Error-correction circuit total gate count (MG)	Timing violation (ns)	Wiring congestion (%)	High-speed cell usage (%)
Target value	-	-	○	2.3W or less	11MG or less	-	-0.01	0.1% or less	10% or less
Method 1	400G per 1blk, 2-parallel configuration	Code A (96)	○	1.92	11.5	54.3	-0.19	39.00	32.36
Method 2	Pipeline decoding processing	Code A (96)	○	2.13	13.4	60.8	-0.54	1.24	29.69
Method 3	Lengthening short code of QC-LDPC code 100G per 1blk, 8-parallel configuration	Code B (64)	△	2.88	10.6	78.6	-0.40	0.10	37.72
Method 4	Reduction of decoding operation bit width of Method 3	Code B (64)	×	2.48	8.9	67.2	-0.27	0.15	30.94
Method 5	Lengthening short code of QC-LDPC code Higher performance of concatenated hard-decision code	Code C (64)	○	2.75	8.7	82.0	-0.11	0.12	22.08
Method 6	Application of 1/2 operating frequency 100G per 1blk, 8-parallel configuration	Code C (64)	○	2.30	10.9	105.2	0	0.09	0.27

to avoid wiring congestion, but the outlook for circuit feasibility was poor, and there was feedback on code design and decoding circuit architecture in terms of code length and circulant matrix size. Finally, all goals were achieved with Method 6, in which optimization of operating frequency is added to the circuit architecture formulated in Method 3 and a redesigned code.

4. Dynamic Power Saving Method Using Decoding Circuit Control Considering Eevice Characteristics

The error-correction decoding circuit increases in scale in proportion to increasing transmission capacity, and there are limits on static power reduction through decoding processing simplification and circuit implementation technology alone. Thus low power must be achieved through dynamic circuit control that takes into account characteristics in terms of equipment operation.

By exploiting the high error-correction performance of QC-LDPC codes used for optical communication, it is possible to tolerate occurrence of errors in transmission paths, and this enables extension of transmission distances. However, when operation of optical communication equipment is considered, it is typical to operate in a range with a certain margin with respect to the error-correction limits. In other words, in actual operating ranges, received signals with higher signal quality than those near the error-correction limit can be obtained, so power consumption can be reduced by monitoring the signal degradation state on a code-by-code basis and dynamically stopping the decoding circuit to avoid unnecessary calculations(3). Figure 3 shows the power reduction effect due to decoding operation control based on signal quality. The horizontal axis indicates the offset SNR (Signal to Noise Ratio), taking the error-correction limits as a basis, and the vertical axis shows normalized power consumption, taking as a basis the power when there is no dynamic stopping of decoding circuits. At the error-correction limits, or on transmission paths with characteristics worse than that (negative side), the error-correction decoding circuits operate constantly, and power consumption approaches 100%. By operating, in contrast, in a range with a margin of at least 0.5dB with respect to error-correction limits, results have been obtained where power consumption can be reduced close to 40% from that at maximum operation.

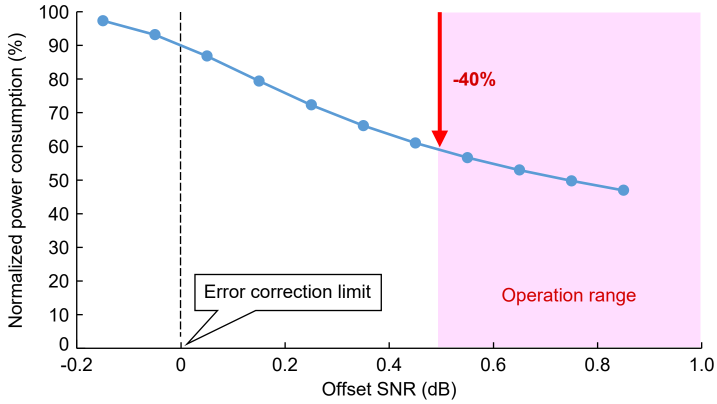

Fig. 3 Power reduction effect by decoding operation control according to signal quality

5. Conclusion

Using the LDPC code for 800Gbps high-capacity optical communications as an example, we described low-power design technology for error-correction circuits using advanced wafer manufacturing processes. As communication networks become larger in capacity, there is a demand for the contradictory characteristics of improved correction performance and low power consumption at the same time. However, the demand for low power consumption can no longer be met by advances in wafer manufacturing processes alone. To achieve these goals, dynamic power saving that takes advantage of the operational characteristics of the equipment described in this paper is likely to become increasingly important.

In addition, while this paper uses the ASIC development of an error-correction circuit for optical communications using advanced wafer manufacturing processes as an example, the same is also valid for FPGA (Field Programmable Gate Array), which is becoming increasingly miniaturized. In FPGA, the circuit resources available for each device are limited, so digital design technology that integrates system/application characteristics with implementation characteristics is important, along with optimization from both the code design and circuit design perspectives.

References

(1) R. G. Gallager: Low density parity check code, Research Monograph series, Cambridge, MIT Press (1963)

(2) Hirano, S., et al.: Design Technology for Improving Performance, Circuit Scale, and Power Consumption in the Backend Phase of LSI Development, Mitsubishi Denki Giho, 96, No. 9 (2022)

(3) Konishi, Y., et al.: High-speed low-power forward error correction coding technology for communications, IEICE Technical Reports, 120, no. 137, PN2020–18 (2020)

River Flow Prediction for Low Flow Management Considering Power Plant Discharge

Author: *Kei Akama**

**Information Technology R&D Center*

Abstract

River administrators are currently carrying out “low flow management” to ensure the river flow necessary for maintaining normal river function by taking steps such as dam discharge. Low flow management establishes, as a target, the normal flow necessary for maintaining normal function of the river. From the standpoint of efficient utilization of water resources, it is also necessary to predict the amount of decline in flow in the future, and appropriately determine the amount of dam discharge. This paper discusses an approach to flow prediction for low flow management—more specifically, the unique features of low flow management in the Arakawa River upstream, the prediction algorithm of the prediction system, and the results of predicting flow using past track record data. The developed prediction algorithm has the following characteristics: (1) It predicts phenomena that can be dealt with such as changes in the amount of dam discharge, and (2) It removes the effects of power plant discharge which are difficult to accurately predict due to lack of data. Using this algorithm, it was confirmed that flow can be predicted with high precision while suppressing upward deviation of prediction, even in the complex water budget environment of the Arakawa River upstream.

1. Introduction

River administration includes both “high flow management” where flood control is performed during flooding, and “low flow management” which involves flowing water management performed in the normal environment or for the purpose of water utilization. In low flow management, the flow necessary for maintaining normal function of the river is stipulated, and that is called the normal flow. More specifically, this flow is made up of the maintenance flow—established in light of factors such as protection of plants and animals, fishing industry, scenic views, and ensuring the cleanliness of flowing water—and the water utilization flow. The flow is established as a target in the context of low flow management. A river administrator must perform management, through steps such as dam discharge, so that river flow does not drop below normal flow(1). From the standpoint of efficient utilization of water resources, it is also necessary to predict the amount of decline in flow in the future, and appropriately determine the amount of dam discharge(2)(3).

In the upstream part of a river, normal flow is set at a water use reference point, with the objective of maintaining normal functions of flowing water such as conserving the river environment—e.g., by preventing the river bed from drying up—and providing stable supply of municipal water, agricultural water, and so on(4). The water use reference point for the Arakawa River upstream is the Yorii point (Saitama Prefecture). Staff currently check flow at the Yorii point day and night, and predict the decline in flow. The amount of dam discharge is determined based on experience, and a discharge instruction is issued. More efficient integrated operation of dams and reduced burden on staff can likely be achieved by automatically calculating the appropriate discharge amount, taking into account information like rainfall and river flow predictions. Therefore, there is a need for a river flow prediction system which can estimate river flow, to serve as the basis for determining the amount of water supplied near the water use reference point.

This paper describes the development situation surrounding a river flow prediction system to support low flow management for the Arakawa River upstream. The purpose of this system is to automatically calculate the decline in flow at the water use reference point, where staff currently make experience-based predictions relying on observation data on dams and river flow, and thereby reduce the burden of low flow management, and improve its efficiency. In accordance with the purpose of low flow management, it was decided in this system to focus on prediction during flow decline, and to deemphasize prediction precision when flow is increasing.

2. Low Flow Management for the Arakawa River Upstream and the Flow Prediction Algorithm for Low Flow Management

This section describes the approach to flow prediction for low flow management, and the algorithm for that prediction. In low flow management, actions must be taken to ensure that that river flow at the water use reference point does not drop below normal flow. Therefore, the conditions where the predicted flow does not exceed the actual flow (i.e., where there is no upward deviation) are taken to be the goal of algorithm review.

Figure 1 shows the river system connections of the Arakawa River upstream. On the Arakawa River, the Arakawa Upstream River Office (the river administrator) determines discharge from the upstream dams so that flow at the Yorii point exceeds the normal flow. Directly above the Yorii point is the Tamayodo Dam. Since the Tamayodo Dam is a facility not subject to integrated management (authority to issue instructions), it was decided to make the Oyahana point (Saitama Prefecture) the flow prediction point. In low flow management, the first step is understanding the recovery situation of reservoir storage based on the influx situation for each dam. Then the flow decline is predicted at the flow prediction point. Efficient low flow management is performed through integrated management of amounts discharged from multiple dams—in Fig. 1, the Futase Dam, Takizawa Dam, and Urayama Dam—while taking into consideration the arrival time of water discharged from each dam at the flow prediction point. However, at present, a flow prediction system for low flow management has not been adopted, and thus operational decisions are dependent on the experience and know-how of skilled staff, and the burden is excessive. In the Arakawa River upstream, the propagation delay time of dam discharge water up to the flow prediction point is roughly 10 hours. Thus, for this prediction system, it was decided to predict flow at the flow prediction point (Oyahana point) up to 12 hours later.

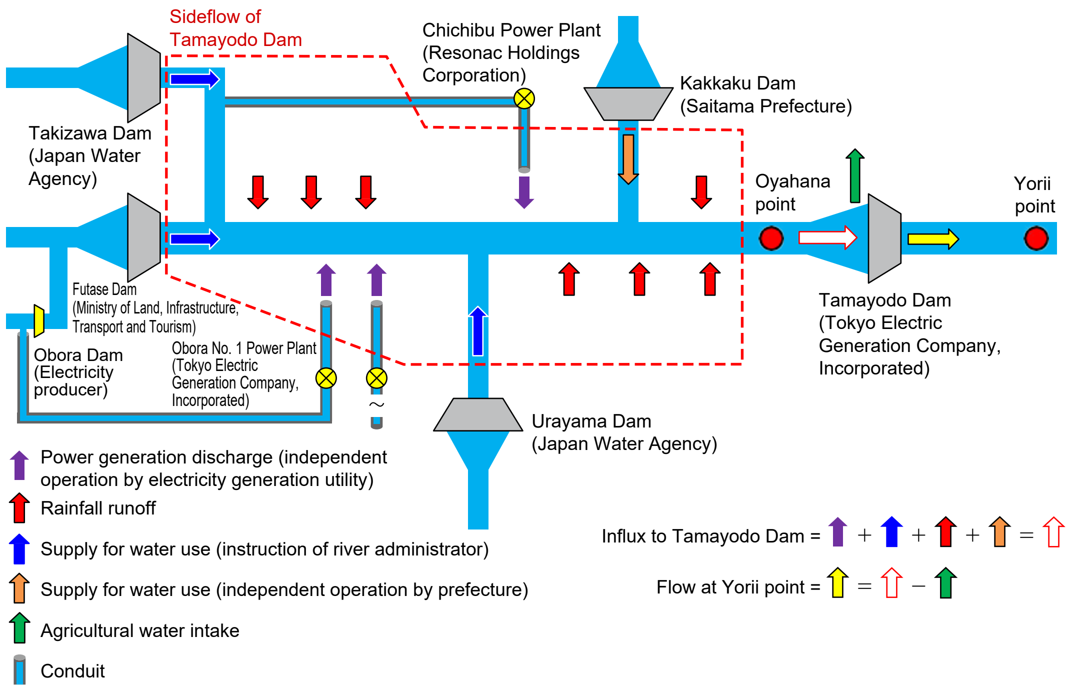

Fig. 1 River system connections of the Arakawa River upstream

Figure 2 shows a conceptual diagram of the effect of power plant discharge. As shown in Fig. 1, there are multiple power plants and conduits in the Arakawa River upstream. The power plant discharge that passes through those facilities is irregularly supplied (returned) to the Arakawa River main stream at intervals of a few hours to a few days, and thus flow at the Oyahana point (the flow prediction point) also varies irregularly. As shown in Fig. 2, what is predicted in this case is the natural flow of the Arakawa River, i.e., the original volume of water in the river without any human interventions, and thus there is a need to separate power plant discharge from the natural flow of the Arakawa River. However, the amount of power plant discharge is determined independently by electricity generation utilities, and data on that discharge is not available. Thus, an approach was considered where flow variation due to power plant discharge, which cannot be predicted, is left out of consideration, and flow variation due to dam discharge, for which data is available, is predicted. For flow variation due to power plant discharge, first the flow inflection points at the prediction point (Oyahana) are extracted, and then the start and end times of the temporary flow variation are estimated. Then the flow between the start and end times is removed by performing linear interpolation. This allows removal of flow variation due to power plant discharge by using only flow data for the flow prediction point.

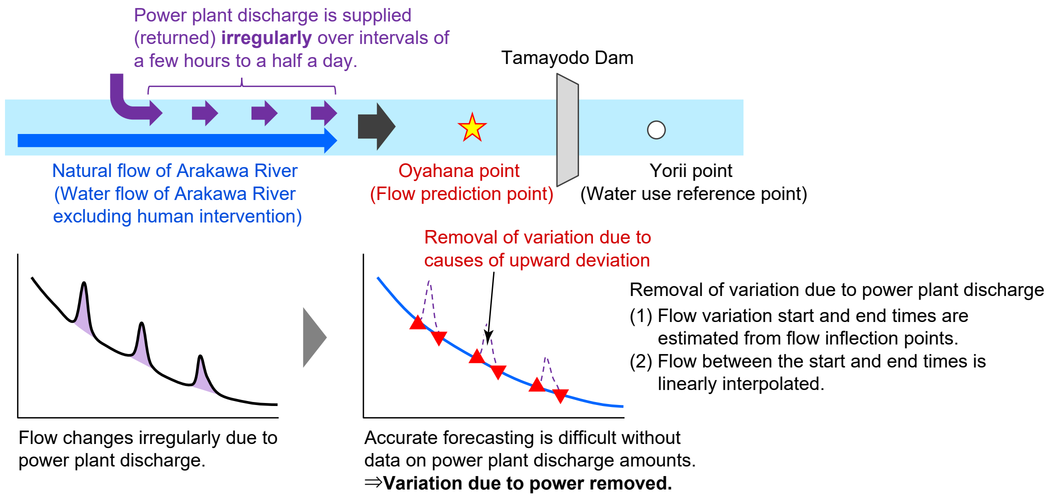

Fig. 2 Effect of power plant discharge

3. Results of Flow Prediction

The actual flow at the flow prediction point (Oyahana point) and the actual discharge of each dam for 2017 to 2022 were input, and flow at the flow prediction point was estimated and predicted using the flow prediction algorithm. Figure 3 shows estimation and prediction results for flow at the flow prediction point. The light blue line in the graph indicates the recorded flow at the flow prediction point, and the red line indicates the estimated/predicted value of the natural flow of the Arakawa river at the flow prediction point. The vertical red dotted line represents the most recent time of the input data. Before that are estimated values, and after that are predicted values. Short-term flow variation due to power plant discharge was removed from the graph, and it was confirmed that estimation and prediction were achieved without the predicted flow (red line) exceeding the recorded flow (blue line). It was also confirmed that flow variation during changes in dam discharge was correctly estimated.

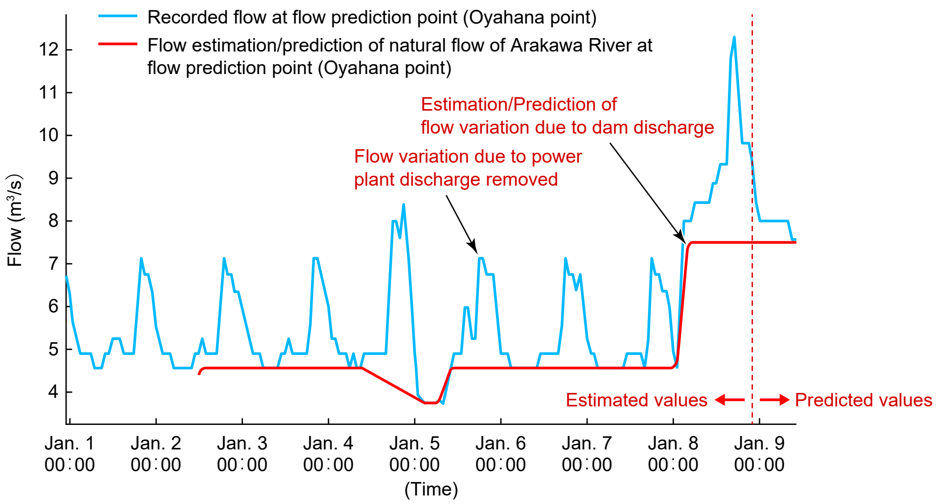

Fig. 3 An example of river flow estimation and prediction

Next, are the results of evaluating prediction error. Evaluation was carried out for an irrigation period (June 18 to July 1) and a non-irrigation period (December 1 to 31). Figure 4 and Fig. 5 show the flow prediction error 12-hours later. The red dotted lines in the graph indicate the range of error with respect to the recorded flow. Upper and lower bounds are +1m^3/s and -2m^3/s respectively. Positive error indicates an upward deviating prediction where the predicted flow exceeds the recorded flow, while negative error indicates a downward deviation. It is evident from the figures that prediction error is almost entirely in the range -2 to +1m^3/s for both the irrigation and non-irrigation period, and flow can be predicted with high precision while suppressing upward deviation of predictions.

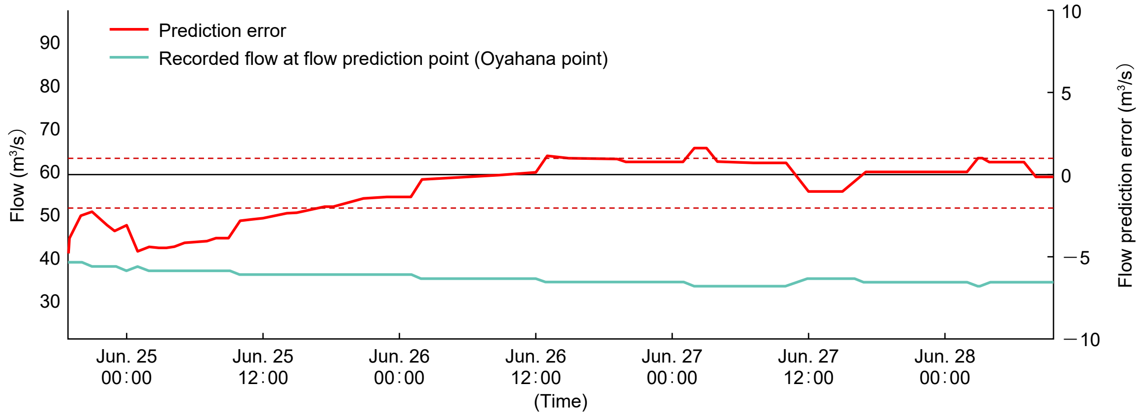

Fig. 4 Error of 12 hours river flow prediction (June 2021)

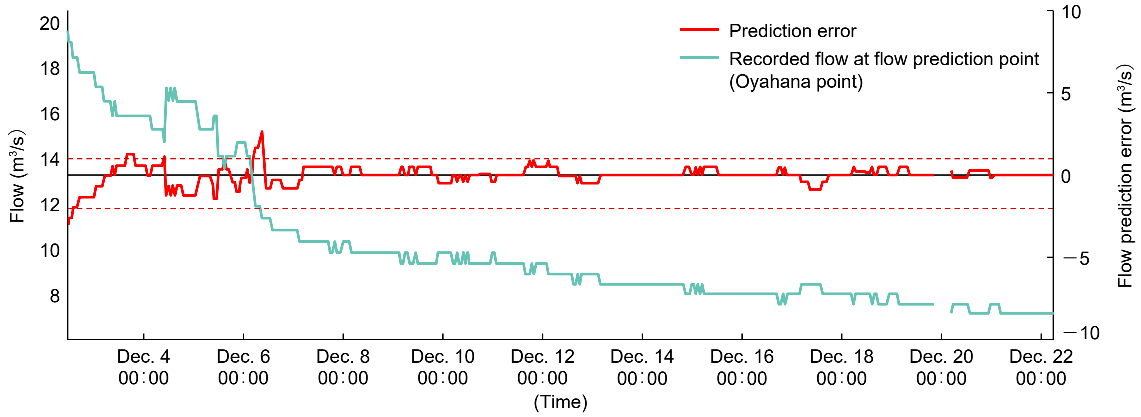

Fig. 5 Error of 12 hours river flow prediction (Dec. 2019)

4. Conclusion

This paper has discussed an approach to flow prediction for low flow management, the unique features of low flow management in the Arakawa River upstream, the prediction algorithm of the prediction system, and the results of predicting flow using past track record data. For low flow management, the predicted flow must not exceed the recorded flow (upward deviation) because the aim of management is to prevent flow at the reference point from dropping below the normal flow. However, in the Arakawa River upstream, a complex water budget is formed by multiple dams, power plants, and conduits, and thus flow at Oyahana (the point for prediction) also varies in a complex way. Therefore, an algorithm was developed to: (1) Predict phenomena that can be dealt with such as changes in the amount of dam discharge, and (2) Remove the effects of power plant discharge that are difficult to accurately predict due to lack of data. Using this algorithm, it was confirmed that flow can be predicted with high precision while minimizing upward deviation in prediction. By using this flow prediction system for low flow management, it will be possible to disperse the load concentrated on skilled staff, and improve the efficiency of low flow management.

References

(1) River Environment Division, River Bureau, Ministry of Land, Infrastructure, Transport and Tourism: Guide for Investigating Normal Flow (draft) (2007)
https://www.mlit.go.jp/river/shishin_guideline/ryuuryoukentou/tebiki.pdf

(2) Kanayama, T., et al.: Field application to low flow integrated management of Tonegawa River upstream dams using AI reinforcement learning, Research Presentations on Construction Consultant Services, 22, 77–80 (2022)

(3) Kanayama, T., et al.: Application of AI reinforcement Learning to Water Management in the Upper Tone River Basin, Journal of Japan Society of Civil Engineers, Ser. B1 (Hydraulic Engineering), 78, No. 2, I_1249 – I_1245 (2022)

(4) Arakawa Upstream River Office, Kanto Regional Development Bureau, Ministry of Land, Infrastructure, Transport and Tourism: Arakawa River Upstream River Maintenance and Management Plan [Volume on Section Managed by the Minister of Land, Infrastructure, Transport and Tourism] (2017)
https://www.ktr.mlit.go.jp/ktr_content/content/000687781.pdf

Terahertz Wave Sensing Technology Supporting Safety and Security

Authors: *Shusaku Umeda*, Ichiro Somada**

**Information Technology R&D Center*

Abstract

Terahertz waves have a frequency between light waves and radio waves. They can realize high-resolution sensing while maintaining transmittance performance, and thus are expected to be used in various applications necessary for achieving safety and security. On the other hand, there are various technical issues for terahertz wave sensing, such as calculation of near field reflection coefficients, and ensuring yield. This paper describes the digital signal processing technology and device technology that serve as core technologies for the 300Ghz-band terahertz wave sensing systems that Mitsubishi Electric is developing. It also presents the results of demonstration experiments that clarify the effectiveness of the terahertz wave sensing system, and shows that it is possible to achieve mm-class imaging and μm-class displacement estimation.

1. Introduction

Light and radio waves have previously been used as media for sensing the shape or movement of target objects present in neighborhood space. For light waves, there are sensors capable of high-resolution sensing, such as cameras and Time of Flight (ToF) sensors. However, it is difficult to sense hidden objects because light waves are highly susceptible to shielding, and are greatly affected by obstacles. Radio waves, on the other hand, have outstanding transmittance properties compared to light waves. However, they have longer wavelengths and thus it is hard to achieve high resolution.

Thus, terahertz waves have attracted attention in recent years as a sensing medium with the characteristics of both light and radio waves. Terahertz waves are electromagnetic waves with a frequency between light waves and radio waves (100Ghz to 10Thz), and they allow sensing even objects behind obstacles with high precision and definition. Therefore, these waves are expected to see application in fields related to safety and security such as imaging applications like body scans and infrastructure inspection, and movement detection applications like infrastructure inspection. While touching on applications where terahertz wave sensing is expected to be used, this paper discusses development and demonstration testing results of our company's sensing technology using 300Ghz-band terahertz waves which will help realize these applications.

2. Sensing System Using Terahertz Band

With this terahertz wave sensing system, sensing is performed through beam-scanning of the target space for measurement, based on the principles of Multiple-Input Multiple-Output (MIMO) radar. With MIMO radar, a signal is sent from a transmission array antenna, and the signal reflected by the measurement target is received by a reception array antenna. Sensing is performed by calculating the reflection coefficient of each part of the measured space from the received signal.

Terahertz waves have high distance attenuation, and a terahertz wave sensing system is assumed to take the neighborhood region (Fresnel zone) as the observation environment, and thus the reflected waves cannot be regarded as far field (plane waves) as in the case of conventional MIMO radar. Therefore, in previous directivity control via beamforming, measurement takes time because focus control is performed according to distance with the antenna element, after identifying coordinates (i.e., the point of interest) in the space to be measured. Manufacturing of array antennas for transmitting and receiving terahertz waves requires microfabrication to arrange antennas at high density, and it is hard to ensure yield during manufacturing. These problems are solved with virtual focus sensing technology and MIMO antennas in a box layout, as shown in Fig. 1.

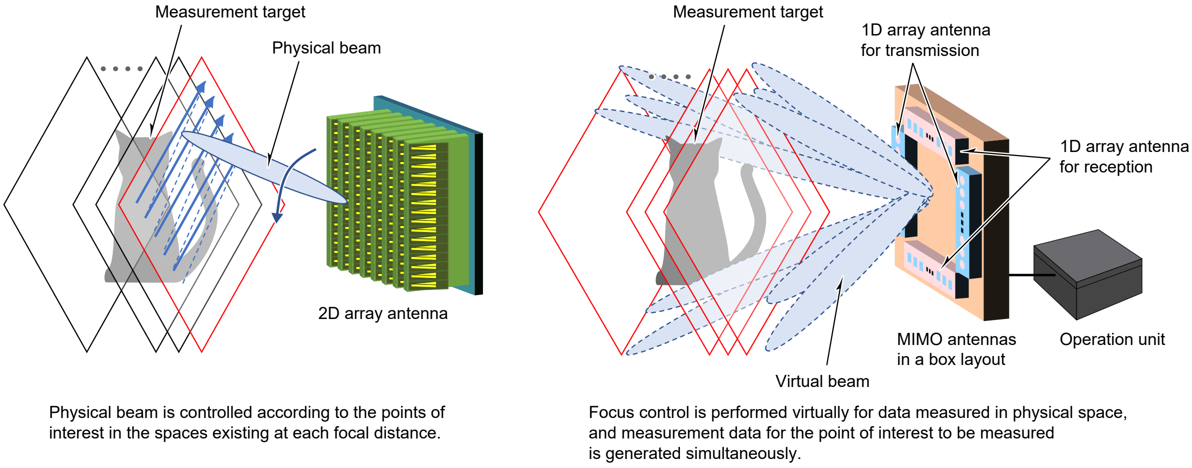

(a) Physical beam sensing + 2D array antenna (conventional technology)

(b) Virtual focus sensing + MIMO antennas in a box layout (developed technology)

Fig. 1 Sensing System Using Terahertz Band

With widely-used 2D array antenna radar, a physical beam with directivity is formed by adjusting signal phases from antenna elements, and the measurement target is sensed while varying the beam direction. Therefore, sensing can only be done for one point of interest at a time. With virtual focus sensing technology, on the other hand, reflected waves are measured without performing directivity control, and multiple points of interest to be measured can be simultaneously sensed by forming a virtual beam focused on those points in a virtual space.

For our terahertz wave sensing system, we have developed a box MIMO antenna arrangement as a MIMO configuration capable of ensuring yield during manufacturing. In this arrangement, 1D array antennas for transmission, with antenna elements placed in a straight line, are arranged in the vertical direction, and 1D array antennas for reception, with the same linear structure, are arranged in the horizontal direction. An equivalent to a 2D array antenna is realized by calculating distance to the point of interest through combination of all of the transmission antenna elements and reception antenna elements, and then estimating the reflection coefficient. Furthermore, by placing the two 1D array antennas for transmission and two 1D array antennas for reception in a box layout, an aperture area is obtained which is equivalent to a high-density layout of antennas in two-dimensions, and this enables high-resolution sensing.

3. Terahertz Wave Device Technology

In order to realize the aforementioned MIMO antenna in a box layout, Mitsubishi Electric has developed 1D array antennas that operate in the 300GHz band. Element technologies needed to realize array antennas can be broadly divided into two categories: (1) radio-frequency integrated circuits (RFIC), and (2) antenna packages. This section presents these technologies owned by Mitsubishi Electric.

Figure 2 shows the composition of the 300GHz-band transmission and reception RFICs we have developed. A 45nm Silicon on Insulator–CMOS (SOI-CMOS) process, promising both good integration performance and higher output, is used for this development.

The transmission and reception RFICs must be lined up at an interval of half wavelength, and high-density layout is required with two systems laid out in 1.15mm or less, as shown in Fig. 2. Due to the unprecedented high- density layout, it is necessary to reduce the number of circuits as much as possible. Therefore, the transmitter RFIC is not configured with two conventional double multiplier stacked on top of each other, but rather with a 0/45deg phase shifter, 75GHz band amplifiers, and a quadruple multiplier as shown in Fig. 2(a), while the receiver RFIC is configured with 75GHz band amplifiers, a quadruple multiplier, and a fundamental wave mixer as shown in Fig. 2(b), forming a 300GHz band transmitter/receiver RFIC with a different circuit configuration than conventional ones.

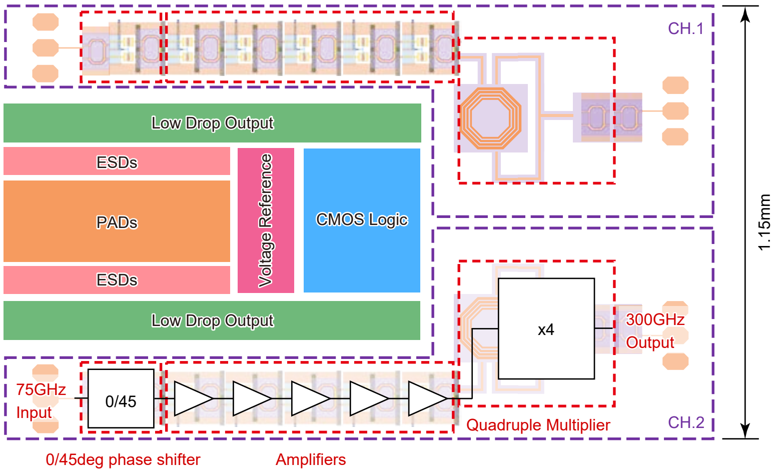

(a) Transmitter RFIC

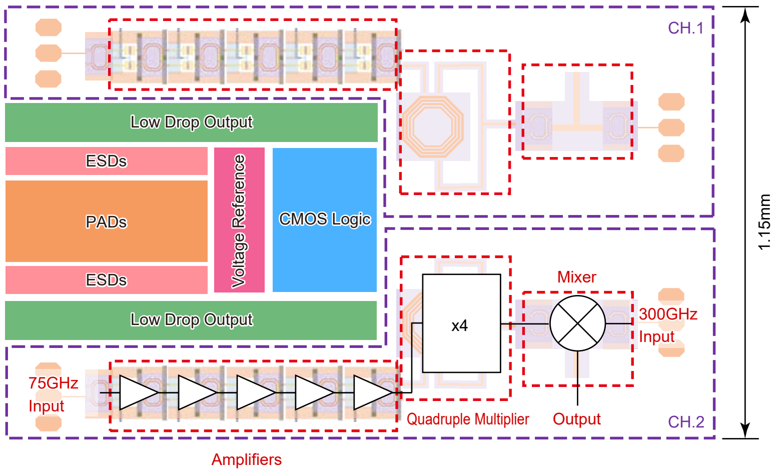

(b) Receiver RFIC

Fig. 2 Configuration of 300GHz band RFIC

The basic configuration of the 300GHz-band antenna package, a prototype drawing, and a prototype sample are shown in Fig. 3. This structure is a dual patch antenna using the redistribution layer process. This process is an IC post-processing technology. The constituent elements are: the IC layer (base material: SiO_2), redistribution layer (RDL), and single-sided film substrate. The antenna fed patch, consisting of a circular patch, is formed on the top layer of the RDL. Power is supplied to the antenna through the backside. This is done via a matching circuit formed on the IC layer by using a feed pin (stack VIA) which connects the IC layer from the RDL.

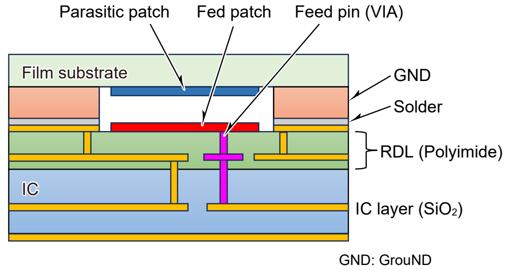

(a) Conceptual illustration of side view

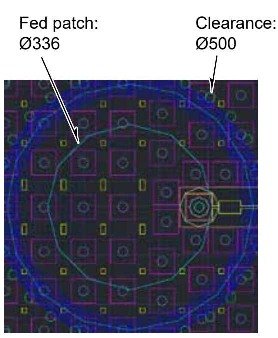

(b) Prototype drawing

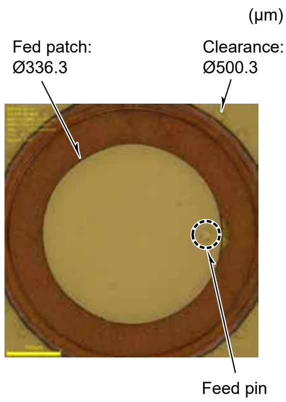

(c) Prototype sample

Fig. 3 Basic configuration of 300GHz band antenna package

The parasitic patch, on the other hand, is formed on the single-sided film substrate, and mounted using conductive tape so that the parasitic patch faces downward. As shown in Fig. 3(b) and (c), a pattern manufacturing error of 1μm or less was achieved for the antenna fed patch as a result of this mounting, and it was confirmed that manufacturing can be done with high precision using this process. The above shows that this method enables high-precision manufacturing and mounting, as well as broader bandwidth due to the use of a dual patch antenna, making it easy to achieve the desired antenna characteristics.

4. Results of Terahertz Wave Sensing Demonstration Experiments

Demonstration experiments on tomographic imaging(1) and vital sensing(2) were carried out to confirm the effectiveness of the 300GHz-band terahertz wave sensing system. Figure 4 shows the measurement system that was used and the results of the measurement. The aforementioned 1D array antennas are currently under development, so a 2D array antenna is simulated by moving a single transmission horn antenna and reception horn antenna placed on an XY stepper, and sensing a stationary body. The inside of a suitcase was filled with expanded polystyrene panels. Then, a toy gun and knife were embedded in separate panels, and tomographic imaging was carried out. The results confirmed that contours and surfaces of the target objects can be imaged with mm precision at the layers where the model gun and knife were respectively placed.

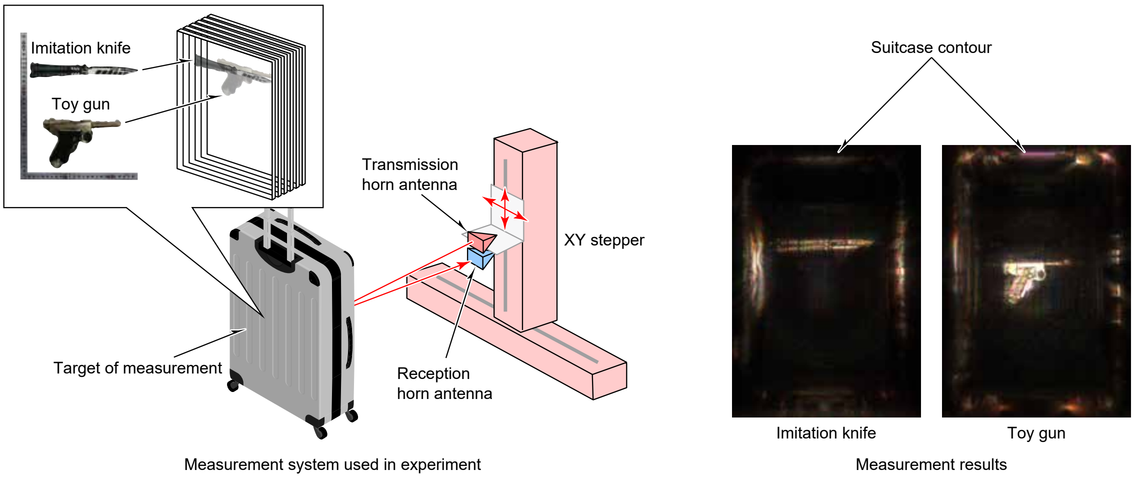

Fig. 4 Results of Tomographic Imaging

Next, vital sensing was carried out as an example of a movement detection application. This involved capturing the pulse information from a human body. Figure 5 shows the measurement image and results. Unlike tomographic imaging, this validation involves sensing a moving body, and thus the experiment was carried out by simulating directivity with a lens. The experiment results confirmed that chest displacement on the order of μm which occurs due to the heartbeat can be estimated, and estimation can be done with an error of 0.5% relative to the electrocardiograms (ECG) used to estimate heartbeat intervals in the medical field.

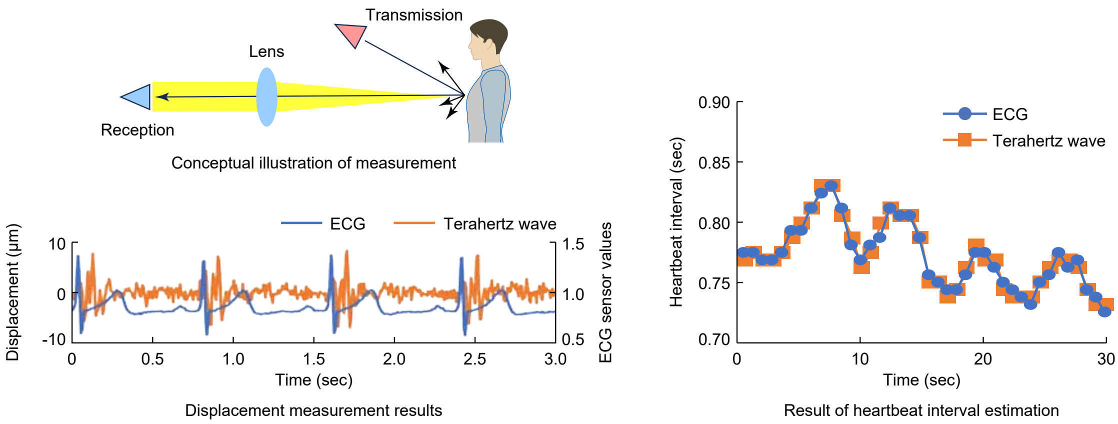

Fig. 5 Result of Vital Sensing Measurement

Based on the above validation, the technology is expected to be used in areas such as nondestructive inspection and infrastructure monitoring, which make use of the characteristics of 300GHz-band terahertz waves.

5. Conclusion

This paper has discussed Mitsubishi Electric's technology and demonstration experiment results for a 300GHz terahertz wave sensing system for realizing high-resolution sensing of hidden objects. It was shown that high resolution and transmittance performance can be achieved with core technologies for 300GHz-band terahertz waves—i.e., virtual focus sensing technology, 300GHz-band RFIC, and packaging technology—and that applications can be expected across a variety of fields, including security gates and vital sensors.

References

(1) Taira, A., et al.: 300GHz band Sub-Terahertz Sensing Technologies for High Resolution Imaging, IEICE Technical Report, 123, no. 76, RCS2023-77, 288–293 (2023)
(2) Umeda, S., et al.: Experimental study of vital sensing using 300GHz band sub-terahertz wave, IEICE Technical Report, 123, no. 108, RCS2023-100, 109–114 (2023)

MITSUBISHI ELECTRIC CORPORATION